AAS 12-237

American Astronautical Society

American Institute of Aeronautics and Astronautics

ATTITUDE STABILIZATION USING NONLINEAR DELAYED ACTUATOR CONTROL WITH AN INVERSE DYNAMICS APPROACH

Morad Nazari, Ehsan Samiei, Eric A. Butcher, and Hanspeter Schaub

AAS/AIAA Space Flight Mechanics Meeting

Charleston, South Carolina January 29 – February 2, 2012

AAS Publications Office, P.O. Box 28130, San Diego, CA 92198

AAS 12-237

ATTITUDE STABILIZATION USING NONLINEAR DELAYED ACTUATOR CONTROL WITH AN INVERSE DYNAMICS APPROACH

Morad Nazari,* Ehsan Samiei,* Eric A. Butcher,† and Hanspeter Schaub‡

The dynamics of a rigid body with nonlinear delayed feedback control are studied in this paper. It is assumed that the time delay occurs in one of the actuators while the other one remains is delay-free. Therefore, a nonlinear feedback controller using both delayed and non-delayed states is sought for the controlled system to have the desired linear closed-loop dynamics which contains a time-delay term using an inverse dynamics approach. First, the closed-loop stability is shown to reduce to a second order linear delay differential equation (DDE) for the MRP attitude coordinate for which the Hsu-Bhatt-Vyshnegradskii stability chart can be used to choose the control gains that result in a stable closed-loop response. An analytical derivation of the boundaries of this chart for the undamped case is shown, and subsequently the Chebyshev spectral continuous time approximation (ChSCTA) method is used to obtain the stable and unstable regions for the damped case. The MATLAB `dde23` function is implemented to obtain the closed-loop response which is in agreement with the stability charts, while the delay-free case is shown to agree with prior results.

NOMENCLATURE

D	Chebyshev spectral differentiation matrix
J	inertia matrix in principal coordinates
$\vec{u}$	feedback control law
V	Lyapunov candidate
$\vec{x}, \vec{y}$	assembled state-space vectors
$\vec{z}$	meta-state vector / assembled state-space vector for the transformed delayed equations
$\vec{\omega}$	angular velocity vector (rad/sec)
$\vec{\sigma}$	modified Rodriguez parameter set
τ	time delay (sec)

INTRODUCTION

The stability analysis of spacecraft attitude dynamics with time delay in the feedback is considered in this study. The existence of time delay in a system would be due to communication delays

* PhD student, Mechanical and Aerospace Engineering Department, New Mexico State University, Las Cruces, NM, 88003, USA.

† Associate Professor, Mechanical and Aerospace Engineering Department, AIAA member, New Mexico State University, Las Cruces, NM, 88003, USA.

‡ Associate Professor, H. Joseph Smead Fellow, Aerospace Engineering Sciences Department, AAS Member, AIAA Associate Fellow, University of Colorado, Boulder, CO, 80309-0431, USA.

including delays in the measurement,[1] or processing delays including delays which occur in the actuators which is studied in this paper.

The attitude modeling problem depends on the choice of attitude parameters (coordinates) to represent the orientation of a rigid body relative to an inertial frame. There are several different attitude parametrizations which can be utilized the governing spacecraft equations, However, for space vehicles it is important to know how to implement the idea of successive Euler angle rotations in the study. Borrowing ideas from the Eulerian motion, a set of four Euler parameters known as quaternions is common in the satellite dynamics analyses. Reduction of the number of Euler parameters from four to three is possible via utilizing other coordinate sets called Rodriguez parameters (RPs), also known as Gibbs parameters, or modified Rodriguez parameters (MRPs), where the latest one is used for the investigations in this paper.

Reaction wheels (RWs) and thrusters are used in different papers to develop tracking control laws.[2,3] Three types of controllers are used by Hall *et al*[2] to globally asymptotically stabilize the closed-loop dynamics of spacecraft. Two of the controllers use thrusters for bang-bang control and RWs to provide the necessary corrections, while the third one uses linear feedback for the RWs and nonlinear feedback for the thrusters. A method is developed by Tsiotras *et al*[3] for controlling the spacecraft attitude while tracking a desired power profile. For this purpose, an arbitrary configuration of four or more RWs is used, and the possibility of having singularity for a general wheel configuration is studied. The implemented torque is decomposed into the null space of the configuration and the space perpendicular to the null space. The torque in the null space is employed for power tracking purposes, and the one perpendicular to the null space is used for attitude control.

Stability analysis of time-delayed systems or delay differential equations (DDEs) is important in many fields of science. New constructions of Lyapunov-Krasovskii (L-K) functionals have been developed for the stability analysis of systems with time delay. A modified L-K functional is developed, in particular, by Chunodkar and Akella[4] for spacecraft attitude stabilization with unknown but bounded delay in the feedback control loop. Exponential stability is obtained for all values of the time delay within the selected bounds. A velocity-free controller is designed by Ailon *et al*[5] for attitude regulation of a rigid spacecraft, where the effects of time-delays in the feedback loop are considered. Then, sufficient conditions for exponential stability are established.

Recently a method has been developed to produce an equivalent system of ODEs known as Chebyshev spectral continuous time approximation (ChSCTA)[6] . ChSCTA can be used for obtaining the time response of the DDE system through analysis of the corresponding ODEs rather than converting the DDE into a map. ChSCTA technique is used by Butcher and Bobrenkov[6] to study the stability of different DDEs including ones with either nonlinearities or multiple delays. The spectral accuracy convergence behavior of this technique is compared with that of other continuous time approximation (CTA) approaches for constant-coefficient DDEs and it is also shown that the obtained results are in agreement with those obtained analytically. Bobrenkov *et al*[7] implement ChSCTA and the Lyapunov-Floquet theory to transform time-periodic DDEs to equivalent constant coefficient ODE systems. The significant advantage of this method is that the discrete delays can be sparsely contained in the extended state vector-matrix formulation. Bobrenkov *et al*[8] apply the method in Ref.[7] to the case of DDEs with discontinuous distributed time delay. They further implement their proposed method to the Mathieu equation with discrete and discontinuous distributed delays with either constant and periodic coefficients.

In this paper, the time delay occurs in the actuators and not in the sensors, where a nonlinear controller is sought for the controlled system to have the desired closed-loop dynamics. Two strategies are considered to utilize delayed feedback in applications. First, we consider multi-actuator control where one actuator is delay-free, while the other one has time delay. This strategy can be applied in desaturation maneuvers, or in order to create a null space by reorienting RWs or CMGs without an attitude maneuver. Second, we consider delay stabilization by introducing an intentional time delay into the actuator in order to stabilize an otherwise unstable closed-loop dynamics without delay.

In the next section the MRP set is introduced, and kinematic differential equations and attitude dynamics of the rigid spacecraft are given. Later, the stability boundaries are investigated analytically for the undamped delayed system, while ChSCTA is implemented to obtain the stability charts of the damped case. For the delayed system, furthermore, MATLAB `dde23` function is applied to obtain the time histories of points arbitrarily picked from the stable and unstable regions. A comparison is made further for the time series obtained for the delayed free case with those in the literature. The simulation results are provided at the end.

MRPS AND ATTITUDE DYNAMICS MODEL

In terms of quaternions, the MRP set is defined as

$$\vec{\sigma} = \frac{\vec{\epsilon}}{1 + \beta_0}, \tag{1}$$

where β_0 is the scalar part of the quaternions, $\vec{\epsilon} = \begin{pmatrix} \beta_1 & \beta_2 & \beta_3 \end{pmatrix}^T$ is the vector part, and the quaternion constraint $\sum_{i=0}^{3} \beta_i^2 = 1$ holds. Figure 1 illustrates how the MRP set $\vec{\sigma}$ is related to the principal angle of rotation and quaternions. In the figure, $\vec{\sigma}^S$ corresponds to the shadow set of MRP set $\vec{\sigma}$, and keeps the norm of MRP always less than or equal to one in order to avoid singularities in the system.

The angular momentum vector about point P is expressed as

$$\vec{H}_P = J\vec{\omega}, \tag{2}$$

where $\vec{\omega}(t) \in \mathcal{R}^3$ represents the angular velocity of the body frame with respect to the inertial frame, and $J \in \mathcal{R}^{3\times 3}$ is the inertia matrix calculated about P. For convenience, all matrices and vectors in this paper are described in the body frame. The kinetic differential equations of spacecraft (also known as the Euler's equations) are based on the reduced form of the angular momentum time derivative taken in the inertial frame

$$\dot{\vec{H}}_P = \vec{L}_P, \tag{3}$$

where $\vec{L}_P$ is the momentum vector about the center of mass P of the spacecraft. Equation (3) is also valid for either any fixed points in the space, those with constant velocities, or those with acceleration vectors passing through the center of mass. The point P, nevertheless, is taken here as the center of mass of the system for attitude realization and analysis of the spacecraft.

Substituting Eq. (2) into (3), and using the transport theorem Euler's equations can be written as

$$J\dot{\vec{\omega}} + \tilde{\omega}J\vec{\omega} = \vec{L}_P \tag{4}$$

which are, in fact, the kinetic differential equations of the spacecraft.

Equations (4) along with the kinematic differential equations in terms of MRPs

$$\dot{\vec{\sigma}} = B(\vec{\sigma})\vec{\omega} \tag{5}$$

specify the governing equations of the system. The nonlinear matrix $B(\vec{\sigma})$ in Eq. (5) is defined as

$$B(\vec{\sigma}) = \left[(1 - \vec{\sigma}^T\vec{\sigma})I_3 + 2\tilde{\sigma} + 2\vec{\sigma}\vec{\sigma}^T\right], \tag{6}$$

where I_3 is the three dimensional identity matrix.

Consider the attitude dynamics of a rigid spacecraft as

$$\begin{aligned} \dot{\vec{\sigma}}(t) &= \frac{1}{4}B(\vec{\sigma}(t))\vec{\omega}(t) \\ \dot{\vec{\omega}}(t) &= -J^{-1}\tilde{\omega}(t)J\vec{\omega}(t) + J^{-1}\vec{u}(t) \end{aligned} \tag{7}$$

where $\vec{\sigma}(t) \in \mathcal{R}^3$ represents the MRP set, and $\vec{u}(t) \in \mathcal{R}^3$ is the control input analogous to the torque vector $\vec{L}_P$ in Eq. (4). The problem is to stabilize the rigid body attitude dynamics using a feedback control law with a single discrete time delay.

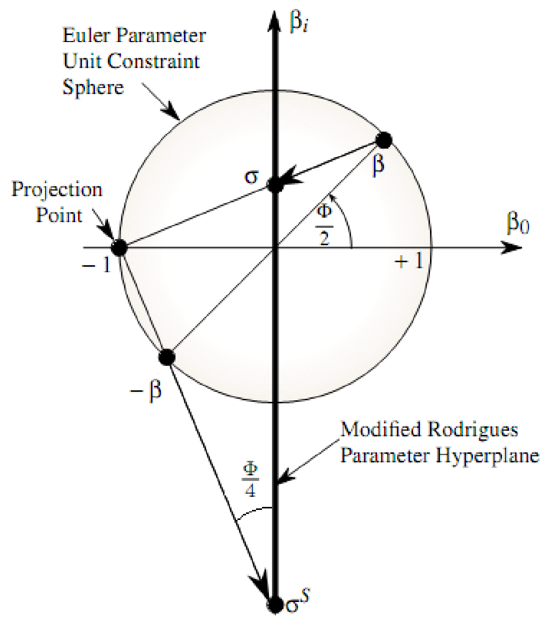

Figure 1. MRP stereographic orientation[9]

ASSUMING THE DESIRED CLOSED-LOOP RESPONSE AND FINDING THE REQUIRED CONTROL LAW

The nonlinearities appearing in Eq. (7) may be viewed as perturbation terms after the linear terms in the equation of motion. There are different approaches for controlling the system with nonlinear terms included. One method is to assume a linear control law which results in a nonlinear model for the closed-loop dynamics of the system[1,5] .Another method is to assume a nonlinear control law which results in a linear model for the closed-loop dynamics of the system[9] . This second approach will be utilized in this section. In particular, an inverse dynamics approach common in robotics open-loop path-planning problems is utilized here, in which the desired closed-loop response is given by a set of second order delay differential equations. This approach (without time delay) has been used in the attitude control problem with both quaternions[10] and MRPs[9] .

Following the method of nonlinear feedback control which results in a linear second order ordinary differential equation (ODE) in terms of the MRPs for the closed-loop dynamics of the delay-free case,[9] we try to include the time delay into the resulting linear equation. This can transform the ODE for the closed-loop dynamics into an analogous DDE. For this purpose, the time delay is assumed to be in the actuators. Hence, we first, following the procedure introduced for the analogue delay-free system, propose the closed-loop equation of the desired controlled system as

$$\ddot{\vec{\sigma}} + P\dot{\vec{\sigma}} + K\vec{\sigma} = R\vec{\sigma}(t-\tau), \tag{8}$$

where P, K, and R are scalars, P and K are preferably positive, and τ is a fixed known time delay. The reason that Eq. (8) is chosen as the desired closed-loop dynamics is that it is a well-known decoupled DDE with a single point delay,[11] and its stability regions can be obtained analytically for the undamped case. In addition, for the damped case, there are some numerical approaches developed in the literature[6,7] to acquire stability diagrams.

Figure 2 gives the schematic block diagram of the system with time delay in the actuators (as opposed to the case where time delay exists in the measurements[1]), where the output can be any of the state vectors of the system or a combination of them. As will be seen, the only way to have time

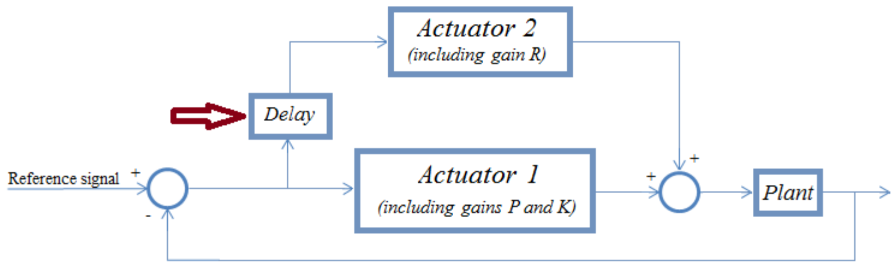

Figure 2. The schematic block diagram of the system with the time delay in one of the actuators

delay in all terms including the MRP set $\vec{\sigma}$ is that the kinematic differential equation of the MRPs include delay terms of $\vec{\sigma}$, since this approach does not apply to the case of having time delay in the feedback controller, and hence, time delay must only be assumed in the actuators. Two strategies are considered to utilize delayed feedback in applications. First, we consider multi-actuator control where actuator (1) is delay-free with gains P and K, while actuator (2) has time delay with gain R as shown in the block diagram in Fig. 2.

Lemma 1 *Based on the desired closed-loop dynamics for the delay-free case,[9] for the delayed system problem, we assume that the desired closed-loop system is*

$$\ddot{\vec{\sigma}}(t) + P\dot{\vec{\sigma}}(t) + K\vec{\sigma}(t) = R\vec{\sigma}(t-\tau), \tag{9}$$

where P and K are positive scalars and R is a scalar. The body angular acceleration vector $\dot{\vec{\omega}}$ can be simplified to

$$\dot{\vec{\omega}} = -P\vec{\omega} - \left[\vec{\omega}\vec{\omega}^T + \left(\frac{4K}{1+\sigma^2} - \frac{\omega^2}{2}\right) I_3\right]\vec{\sigma} + 4B^{-1}R\vec{\sigma}(t-\tau). \tag{10}$$

Proof 1 *Differentiating both sides of the first equation in (7) and substituting the result back into Eq. (9) yields*

$$\ddot{\vec{\sigma}} + P\dot{\vec{\sigma}} + K\vec{\sigma} = \frac{1}{4}B\left[\dot{\vec{\omega}} + P\vec{\omega} + B^{-1}(\dot{B}\vec{\omega} + 4K\vec{\sigma})\right] = R\vec{\sigma}(t-\tau). \tag{11}$$

Knowing that B^{-1} always exists for $\sigma < 1$ with $\sigma := \|\vec{\sigma}\|$, Eq. (11) becomes[9]

$$\dot{\vec{\omega}} + P\vec{\omega} + B^{-1}(\dot{B}\vec{\omega} + 4K\vec{\sigma}) = 4B^{-1}R\vec{\sigma}(t-\tau). \tag{12}$$

Taking the time derivative of matrix B in Eq. (6)

$$\dot{B} = \left(-\dot{\vec{\sigma}}^T\vec{\sigma} - \vec{\sigma}^T\dot{\vec{\sigma}}\right) I_3 + \dot{\tilde{\sigma}} + 2\dot{\vec{\sigma}}\vec{\sigma}^T + 2\vec{\sigma}\dot{\vec{\sigma}}^T \tag{13}$$

$$\dot{\vec{\sigma}}^T = \frac{1}{4}\vec{\omega}^T\left[(1-\sigma^2)I_3 - 2\tilde{\sigma} + 2\vec{\sigma}\vec{\sigma}^T\right] \tag{14}$$

On the other hand,

$$\tilde{\sigma}^2 = \vec{\sigma}\vec{\sigma}^T - \sigma^2 I_3 = \vec{\sigma}\vec{\sigma}^T - \vec{\sigma}^T\vec{\sigma} I_3 \tag{15}$$

Taking the time derivative of both sides of Eq. (15) we obtain

$$\tilde{\sigma}\dot{\tilde{\sigma}} + \dot{\tilde{\sigma}}\tilde{\sigma} = \dot{\vec{\sigma}}\vec{\sigma}^T + \vec{\sigma}\dot{\vec{\sigma}}^T - \left(\dot{\vec{\sigma}}^T\vec{\sigma} + \vec{\sigma}^T\dot{\vec{\sigma}}\right) I_3 = \mathcal{B}, \tag{16}$$

and calling

$$\mathcal{A} := \tilde{\sigma}\dot{\tilde{\sigma}}, \quad \mathcal{A}^T := \dot{\tilde{\sigma}}\tilde{\sigma} \tag{17}$$

Eq. (16) can be written as

$$\mathcal{A} + \mathcal{A}^T = \mathcal{B}. \tag{18}$$

Furthermore,

$$\mathcal{A} - \mathcal{A}^T = \begin{pmatrix} 0 & \sigma_2\dot{\sigma}_1 - \sigma_1\dot{\sigma}_2 & \dot{\sigma}_1\sigma_3 - \sigma_1\dot{\sigma}_3 \\ \dot{\sigma}_2\sigma_1 - \sigma_2\dot{\sigma}_1 & 0 & \dot{\sigma}_2\sigma_3 - \dot{\sigma}_3\sigma_2 \\ \dot{\sigma}_3\sigma_1 - \sigma_3\dot{\sigma}_1 & \dot{\sigma}_3\sigma_2 - \sigma_3\dot{\sigma}_2 & 0 \end{pmatrix} = \dot{\vec{\sigma}}\vec{\sigma}^T - \vec{\sigma}\dot{\vec{\sigma}}^T = \mathcal{C}. \tag{19}$$

Equations (16) and (19) can be solved for $\mathcal{A}$ and $\mathcal{A}^T$

$$\begin{aligned} \tilde{\sigma}\dot{\tilde{\sigma}} = \mathcal{A} = \frac{1}{2}(\mathcal{B}+\mathcal{C}) = &\quad \dot{\vec{\sigma}}\vec{\sigma}^T - \frac{1}{2}\left(\dot{\vec{\sigma}}^T\vec{\sigma} + \vec{\sigma}^T\dot{\vec{\sigma}}\right) I_3, \\ \dot{\tilde{\sigma}}\tilde{\sigma} = \mathcal{A}^T = &\quad \vec{\sigma}\dot{\vec{\sigma}}^T - \frac{1}{2}\left(\vec{\sigma}^T\dot{\vec{\sigma}} + \dot{\vec{\sigma}}^T\vec{\sigma}\right) I_3, \end{aligned} \tag{20}$$

Also note that

$$B^T = \left(1+\sigma^2\right)^2 B^{-1} \tag{21}$$

As is shown in Eq. (13), $\dot{B}\vec{\omega}$ has a term $\dot{\tilde{\sigma}}\vec{\omega}$ which is the hardest term to calculate. But, Eq. (14) implies that

$$\vec{\omega} = 4B^{-1}\dot{\vec{\sigma}} = \frac{4B^T}{\left(1+\sigma^2\right)^2}\dot{\vec{\sigma}}. \tag{22}$$

Hence

$$\dot{\tilde{\sigma}}\vec{\omega} = \dot{\tilde{\sigma}}\frac{4B^T}{(1+\sigma^2)^2}\dot{\vec{\sigma}} = \frac{4}{(1+\sigma^2)^2}\left[(1-\sigma)^2\dot{\tilde{\sigma}}\dot{\vec{\sigma}} - 2\dot{\tilde{\sigma}}\tilde{\sigma}\dot{\vec{\sigma}} + 2\dot{\tilde{\sigma}}\vec{\sigma}\vec{\sigma}^T\dot{\vec{\sigma}}\right] \tag{23}$$

first term of which inside the brackets is zero. According to Eq. (15),

$$2\dot{\tilde{\sigma}}\left(\vec{\sigma}\vec{\sigma}^T\right)\dot{\tilde{\sigma}} = 2\dot{\tilde{\sigma}}\left(\tilde{\sigma}^2 + \vec{\sigma}^T\vec{\sigma}I_3\right)\dot{\tilde{\sigma}} = 2\left(\dot{\tilde{\sigma}}\tilde{\sigma}\right)\left(\tilde{\sigma}\dot{\tilde{\sigma}}\right) + 2\left(\vec{\sigma}^T\vec{\sigma}\right)\left(\dot{\tilde{\sigma}}\dot{\tilde{\sigma}}\right) = 2\left(\dot{\tilde{\sigma}}\tilde{\sigma}\right)\left(\tilde{\sigma}\dot{\tilde{\sigma}}\right). \tag{24}$$

Equation (23) can thus be written as

$$\dot{\tilde{\sigma}}\vec{\omega} = \frac{4}{(1+\sigma^2)^2}\left(-2\dot{\tilde{\sigma}}\tilde{\sigma}\dot{\tilde{\sigma}} + 2\dot{\tilde{\sigma}}\tilde{\sigma}\tilde{\sigma}\dot{\tilde{\sigma}}\right) = \frac{8\dot{\tilde{\sigma}}\tilde{\sigma}}{(1+\sigma)^2}\left(-I_3+\tilde{\sigma}\right)\dot{\tilde{\sigma}} = -\frac{2\dot{\tilde{\sigma}}\tilde{\sigma}}{1+\sigma^2}\left(I_3+\tilde{\sigma}\right)\vec{\omega}. \tag{25}$$

However, substituting for $\dot{\tilde{\sigma}}\tilde{\sigma}$ from Eq. (20) into Eq. (25) we obtain

$$\begin{aligned}
\dot{\tilde{\sigma}}\vec{\omega} = & -\frac{2}{1+\sigma^2}\left[\vec{\sigma}\dot{\vec{\sigma}}^T - \frac{1}{2}\left(\vec{\sigma}^T\dot{\vec{\sigma}} + \dot{\vec{\sigma}}^T\vec{\sigma}\right)I_3\right]\left(I_3+\tilde{\sigma}\right)\vec{\omega} \\
= & \frac{2}{1+\sigma^2}\left(-\vec{\sigma}\dot{\vec{\sigma}}^T + \vec{\sigma}^T\dot{\vec{\sigma}}I_3\right)\left(I_3+\tilde{\sigma}\right)\vec{\omega} \\
= & \frac{1}{2\left(1+\sigma^2\right)}\{(\sigma^2-1)\omega^2\vec{\sigma} + (1+\sigma^2)(\vec{\sigma}^T\vec{\omega})\vec{\omega} - 2(\sigma^2\omega^2)\vec{\sigma} - \\
& (1+\sigma^2)(\vec{\sigma}^T\vec{\omega})\tilde{\omega}\vec{\sigma}\},
\end{aligned} \tag{26}$$

where $\omega := ||\vec{\omega}||$.

Other terms in Eq. (13) are easier to find

$$\dot{\vec{\sigma}}^T\vec{\sigma} = \vec{\sigma}^T\dot{\vec{\sigma}} = \frac{1}{4}\vec{\sigma}^TB\vec{\omega} = \frac{1}{4}(1+\sigma^2)(\vec{\sigma}^T\vec{\omega}), \tag{27}$$

$$\begin{aligned}
2\dot{\vec{\sigma}}(\vec{\sigma}^T\vec{\omega}) = & \frac{1}{2}\left[(1-\sigma^T)I_3 + 2\tilde{\sigma} + 2\vec{\sigma}\vec{\sigma}^T\right](\vec{\sigma}^T\vec{\omega})\vec{\omega} \\
= & \frac{1}{2}(1-\sigma^2)(\vec{\sigma}^T\vec{\omega})\vec{\omega} - (\vec{\sigma}^T\vec{\omega})\tilde{\omega}\vec{\sigma} + (\vec{\sigma}^T\vec{\omega})^2\vec{\sigma},
\end{aligned} \tag{28}$$

and

$$\begin{aligned}
2\vec{\sigma}\dot{\vec{\sigma}}^T\vec{\omega} = & \frac{1}{2}\vec{\sigma}\vec{\omega}^T\left[(1-\sigma^2)I_3 - 2\tilde{\sigma} + 2\vec{\sigma}\vec{\sigma}^T\right]\vec{\omega} \\
= & \frac{1}{2}(1-\sigma^2)\omega^2\vec{\sigma} + \vec{\sigma}\vec{\omega}^T\tilde{\omega}\vec{\sigma} + (\vec{\sigma}^T\vec{\omega})^2\vec{\sigma}.
\end{aligned} \tag{29}$$

Substituting Eqs. (26), (27), (28), and (29) into Eq. (13) yields

$$\dot{B}\vec{\omega} = -2(\vec{\sigma}^T\vec{\omega})\tilde{\omega}\vec{\sigma} + 2(\vec{\sigma}^T\vec{\omega})^2\vec{\sigma} - \frac{1}{2}(1+\sigma^2)\omega^2\vec{\sigma} + (1-\sigma^2)(\vec{\sigma}^T\vec{\omega})\vec{\omega}. \tag{30}$$

Substituting Eq. (30) into Eq. (12) yields

$$\begin{aligned}
\dot{\vec{\omega}} = & -P\vec{\omega} - \frac{1}{\left(1+\sigma^2\right)^2}[-2(1-\sigma^2)(\vec{\sigma}^T\vec{\omega})\tilde{\omega}\vec{\sigma} + 2(1-\sigma^2)(\vec{\sigma}^T\vec{\omega})^2\vec{\sigma} \\
& -\frac{1}{2}1+\sigma^2(1-\sigma^2)\omega^2\vec{\sigma} + (1-\sigma^2)^2(\vec{\sigma}^T\vec{\omega})\vec{\omega} + 4K(1-\sigma^2)\vec{\sigma} + 4(\vec{\sigma}^T\vec{\omega})\tilde{\sigma}\tilde{\omega}\vec{\sigma} \\
& -2(1-\sigma^2)(\vec{\sigma}^T\vec{\omega})\tilde{\sigma}\vec{\omega} + 4(\vec{\sigma}^T\vec{\omega})^2\sigma^2\vec{\sigma} - (1+\sigma^2)\omega^2\sigma^2\vec{\sigma} + 2(1-\sigma^2)(\vec{\sigma}^T\vec{\omega})^2\vec{\sigma} + \\
& 8K\sigma^2\vec{\sigma}] + 4B^{-1}R\vec{\sigma}(t-\tau)
\end{aligned} \tag{31}$$

The term $4(\vec{\sigma}^T\vec{\omega})\tilde{\sigma}\tilde{\omega}\vec{\sigma}$ in Eq. (31) is expressed as

$$-4(\vec{\sigma}^T\vec{\omega})\tilde{\sigma}^2\vec{\omega} = -4(\vec{\sigma}^T\vec{\omega})(\vec{\sigma}\vec{\sigma}^T - \vec{\sigma}^T\vec{\sigma}I_3)\vec{\omega} = -4(\vec{\sigma}^T\vec{\omega})^2\vec{\sigma} + 4(\vec{\sigma}^T\vec{\omega})\sigma^2\vec{\omega}. \tag{32}$$

Substituting Eq. (32) into Eq. (31) yields

$$\begin{aligned}
\dot{\vec{\omega}} = \quad & -P\vec{\omega} - \frac{1}{(1+\sigma^2)^2}[(\vec{\sigma}^T\vec{\omega})^2\vec{\sigma}(2-2\sigma^2+2-2\sigma^2-4+4\sigma^2) \\
& +(\vec{\sigma}^T\vec{\omega})\vec{\omega}(1-2\sigma^2+\sigma^4+4\sigma^2) + \omega^2\vec{\sigma}(-\frac{1}{2}+\frac{\sigma^4}{2}-\sigma^2-\sigma^4)+ \\
& K\vec{\sigma}(4-4\sigma^2+8\sigma^2)] + 4B^{-1}R\vec{\sigma}(t-\tau) \\
= \quad & -P\vec{\omega} - \frac{1}{(1+\sigma^2)^2}\left[\vec{\omega}(\vec{\omega}^T\vec{\sigma})(1+\sigma^2)^2 - \frac{1}{2}(1+\sigma^2)^2\omega^2\vec{\sigma} + 4K(1+\sigma^2)\vec{\sigma}\right]+ \\
& 4B^{-1}R\vec{\sigma}(t-\tau) \\
= \quad & -P\vec{\omega} - \left[\vec{\omega}\vec{\omega}^T + \left(\frac{4K}{1+\sigma^2} - \frac{\omega^2}{2}\right)I_3\right]\vec{\sigma} + 4B^{-1}R\vec{\sigma}(t-\tau).
\end{aligned} \tag{33}$$

The proof is, therefore, complete. □

Equation (9) is written in the state-space form as

$$\vec{x}_1 = \vec{\sigma}, \quad \vec{x}_2 = \dot{\vec{\sigma}}, \quad \vec{x} = \left\{ \begin{array}{c} \vec{\sigma} \\ \dot{\vec{\sigma}} \end{array} \right\} \tag{34}$$

$$\dot{\vec{x}} = \left\{ \begin{array}{c} \dot{\vec{\sigma}} \\ \ddot{\vec{\sigma}} \end{array} \right\} = \begin{pmatrix} 0_3 & I_3 \\ -KI_3 & -PI_3 \end{pmatrix} \left\{ \begin{array}{c} \vec{\sigma}(t) \\ \dot{\vec{\sigma}}(t) \end{array} \right\} + \begin{pmatrix} 0_3 & 0_3 \\ RI_3 & 0_3 \end{pmatrix} \left\{ \begin{array}{c} \vec{\sigma}(t-\tau) \\ \dot{\vec{\sigma}}(t-\tau) \end{array} \right\}. \tag{35}$$

Although, according to Eqs. (35) and (9), 6 DDEs are sufficient to acquire the dynamics behavior of the closed-loop system, in order to include the plots for the time histories of the control signals ($\vec{u}$), as well, the system and the controller are modeled by 9 simultaneous DDEs in the MATLAB `dde23`. Considering the second equation in (7) and Eq. (10) the following nonlinear relation for $\vec{u}(t)$ is obtained

$$\begin{aligned}
\vec{u}(t) = \quad & \tilde{\omega}(t)J\vec{\omega}(t) - JP\vec{\omega}(t) - J\left[\vec{\omega}(t)\vec{\omega}(t)^T + \left(\frac{4K}{1+\sigma^2(t)} - \frac{\omega^2(t)}{2}\right)I_3\right]\vec{\sigma}(t) + \\
& 4J\frac{1}{(1+\sigma^2(t))^2}B^T(t)R\vec{\sigma}(t-\tau),
\end{aligned} \tag{36}$$

where Eq. (21) is used to obtain the expression for the controller.

It is instructive to compare our controller with the standard MRP-based control law[9] using the Lyapunov function

$$V(\vec{\omega}) = \frac{1}{2}\vec{\omega}^T\boldsymbol{J}\vec{\omega} + 2\mathcal{K}\ln\left(1+\vec{\sigma}^T\vec{\sigma}\right). \tag{37}$$

Taking the derivative along the trajectory and forcing it to be negative semidefinite as

$$\dot{V} = \vec{\omega}^T\left(\boldsymbol{J}\frac{{}^{\mathcal{B}}d}{dt}\vec{\omega} + \mathcal{K}\vec{\sigma}\right) = -\vec{\omega}^T\mathcal{P}\vec{\omega} \tag{38}$$

the corresponding asymptotic stabilizing control law[9] for regulation control is obtained as

$$\vec{u}(t) = \tilde{\boldsymbol{\omega}}(t)\boldsymbol{J}\vec{\omega}(t) - \mathcal{P}\vec{\omega}(t) - \mathcal{K}\vec{\sigma}(t). \tag{39}$$

However, the resulting closed-loop dynamics

$$\boldsymbol{J}\frac{{}^{\mathcal{B}}d}{dt}\vec{\omega} + \mathcal{P}\vec{\omega} + \mathcal{K}\vec{\sigma} = \vec{0}, \tag{40}$$

where the superscript $\mathcal{B}$ indicates the time derivative with respect to the body frame, is not linear due to the nonlinearities in Eq. (5). However, the inverse dynamics based control law given in Eq. (36) which has additional quadratic terms compared to the Lyapunov based control law in Eq. (39) does in fact lead to a linear closed-loop dynamics.

In order to further analyze the closed-loop dynamics in Eq. (8), the time is nondimensionalized as

$$t^* = \frac{t}{\tau}, \quad \frac{d}{dt} = \frac{dt^*}{dt}\frac{d}{dt^*} = \frac{1}{\tau}\frac{d}{dt^*}, \quad \frac{d^2}{dt^2} = \frac{dt^*}{dt}\frac{d}{dt^*}\left(\frac{1}{\tau}\frac{d}{dt^*}\right) = \frac{1}{\tau^2}\frac{d^2}{dt^{*2}} \tag{41}$$

Using the transformation Eq. (41) in Eq. (8), the latter becomes

$$\vec{\sigma}'' + \tau P\vec{\sigma}' + \tau^2 K\vec{\sigma} = \tau^2 R\vec{\sigma}(t^* - 1), \tag{42}$$

which, considering the fact that P and K are scalars, can be written as three second order scalar DDEs

$$\sigma_i'' + \bar{P}\sigma_i' + \bar{K}\sigma_i = \bar{R}\sigma_i(t^* - 1), \quad i = 1, 2, 3 \tag{43}$$

where prime and double prime " $'$ "and " $''$ "represent for the first and second derivatives of the dimensionless parameter σ_i with respect to t^*, respectively, and $\bar{P} = \tau P$, $\bar{K} = \tau^2 K$, and $\bar{R} = \tau^2 R$. Introducing the state-space variables in a similar manner as what we had in Eq. (34) for each i

$$z_1 = \sigma_i, \quad z_2 = \sigma_i'. \quad i = 1, 2, 3 \tag{44}$$

Equation (42) can then be written in the state-space form

$$\vec{z}' = \mathbf{A}\vec{z}(t^*) + \mathbf{B}\vec{z}(t^* - 1), \tag{45}$$

where

$$\vec{z} = \begin{Bmatrix} z_1 \\ z_2 \end{Bmatrix}, \quad \mathbf{A} = \begin{pmatrix} 0 & 1 \\ -\bar{K} & -\bar{P} \end{pmatrix}, \quad \mathbf{B} = \bar{R}\begin{pmatrix} 0 & 0 \\ 1 & 0 \end{pmatrix} \tag{46}$$

Two methods, an analytical approach and a numerical approach based on ChSCTA, are further implemented to study the stability of the closed-loop system. The analytical approach only applies to the time delay problem (45) for $\bar{P} = 0$ which can be referred to as the undamped case.

Analytical Investigation for the Undamped Case

Setting $\bar{P} = 0$ in Eq. (42), its corresponding characteristic equation can be written as

$$s^2 + \bar{K} - \bar{R}e^{-s} = 0. \tag{47}$$

Since unstable systems have eigenvalues with positive real parts, s must be set equal to 0 and $i\omega$ to obtain stability boundaries. If one sets $s = 0$ Eq. (47) yields the divergence stability boundary as

$$\bar{K} = \bar{R}, \tag{48}$$

while setting $s = i\omega$ for $\omega \in \mathcal{R}$, and separation of the real and imaginary parts yield

$$\begin{aligned} &-\omega^2 + \bar{K} - \bar{R}\cos\omega = 0, \\ &\bar{R}\sin\omega = 0. \end{aligned} \tag{49}$$

Second equation in (49) yields

$$\sin\omega = 0, \text{ or } \bar{R} = 0. \tag{50}$$

Solving Eqs. (50) and (49) simultaneously yields the flutter (Hopf) stability boundaries as

$$D = D_1 \cup D_2, \tag{51}$$

where

$$\begin{aligned} D_1 &= \left\{(\bar{K}, \bar{R}) |\, \bar{R} = 0,\ \bar{K} > 0\right\}, \\ D_2 &= \left\{(\bar{K}, \bar{R}) |\, \bar{K} - \bar{R}(-1)^n = n^2\pi^2\right\},\ n = 0, 1, 2, \cdots \end{aligned} \tag{52}$$

This stability chart for the undamped case with straight lines, which is shown in Fig. 3 is known as the *Hsu-Bhatt-Vyshnegradskii* stability chart in the literature.[11]

Corollary 1 *The trivial solution of the DDE (43) is exponentially asymptotically stable if and only if there exists an integer $n_1 \geq 0$ such that either*

$$\bar{R} > 0, \quad \bar{R} < \bar{K} - (2n_1)^2\pi^2, \text{ and } \bar{R} < -\bar{K} + (2n_1 + 1)^2\pi^2 \tag{53}$$

or

$$\bar{R} < 0, \quad \bar{R} > -\bar{K} + (2n_1 + 1)^2\pi^2, \text{ and } \bar{R} > \bar{K} - (2n_1 + 2)^2\pi^2, \tag{54}$$

Proof 2 *Since the divergence boundary $\bar{K} = \bar{R}$ is delay independent,[12] for the system without the time delay Eq. (49) becomes*

$$s^2 = \bar{R} - \bar{K} \tag{55}$$

which results in the stable behavior for $0 \leq \bar{R} < \bar{K}$ for the undamped system. Hence the region inside the triangle $\triangle CDE$ is stable. On the other hand, by crossing through the divergence and Hopf stability boundaries the number of unstable characteristic exponents (α) increases by one and two, respectively (see Fig. 3). Since inside $\triangle CDE$ is stable with $\alpha = 0$, starting from a point inside this triangle, if we cross through segment CD (which is the Hopf stability boundary) towards outside of that triangle, the parameter α increases by 2, which means that we are in the unstable region. Now if we move from a point on this unstable region towards inside $\triangle DFG$ by crossing the segment DF, α decreases by 2 again and becomes zero which implies that inside $\triangle DFG$ is also stable. The same strategy can be followed for the other triangles. □

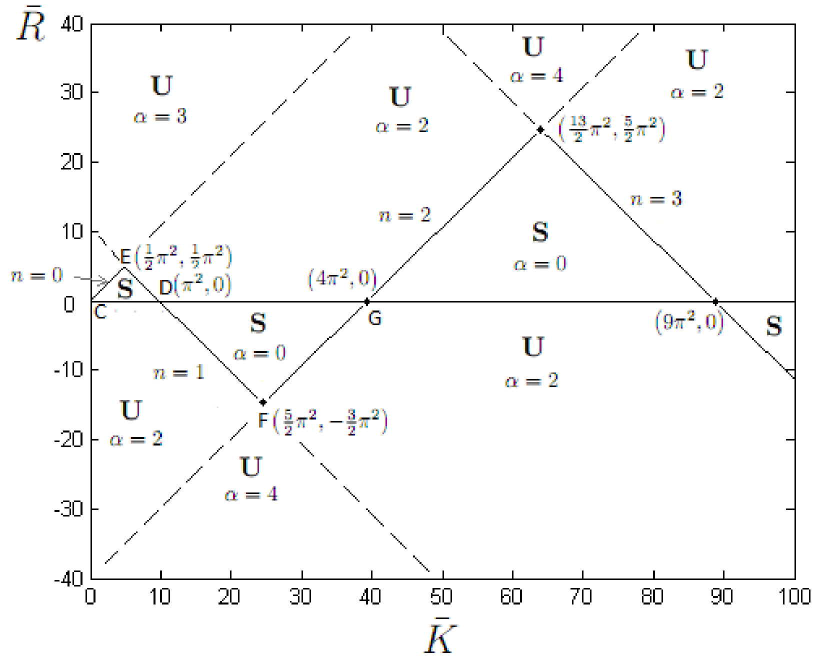

Figure 3. Hsu-Bhatt-Vyshnegradskii stability chart in $\bar{K} - \bar{R}$ plane for $\bar{P} = 0$ obtained analytically.

The first set of conditions given in the Corollary 1 (Eq. 53) gives the stable triangles above the $\bar{R}$ axis, while the second set (Eq. 54) produces the stable triangles below that axis. Figure 3 represents the stability chart obtained analytically in the $\bar{K} - \bar{R}$ plane. The intersections of the first three consequent pairs of lines given in the set D_2 in Eq. (52) are obtained analytically and represented in Fig. 3 along with the crossing points of the lines with the $\bar{K}$ axis.

ChSCTA Method for the Damped Case

For the case $\bar{P} \neq 0$, the characteristic equation is

$$s^2 + \bar{P}s + \bar{K} - \bar{R}e^{-s} = 0, \tag{56}$$

which, after setting $s = j\omega$ and separating real and imaginary parts, yields

$$\begin{aligned} -\omega^2 + \bar{K} - \bar{R}\cos\omega &= 0 \\ \bar{P}\omega + \bar{R}\sin\omega &= 0. \end{aligned} \tag{57}$$

It can be seen that the flutter stability boundaries for this case do not remain as straight lines. However, like the undamped case, the $\bar{K} = \bar{R}$ line can be seen to still correspond to the divergence (fold) instability. We now describe a numerical method used to investigate the stability of this case.

Chebyshev collocation points can be introduced as the projections of the equispaced points on the upper half of the unit circle onto the horizontal axis, mathematically[8]

$$t_i = \cos\frac{i\pi}{N}. \tag{58}$$

where N is the number of the selected points on the semicircle. In the ChSCTA method, the interval $[x(t-\tau), x(t)]$ is broken into $N = m-1$ subintervals lengths of which are determined based on the positions of Chebyshev collocation points, where m is the number of Chebyshev collocation points. The scaling factor $\frac{2}{\tau}$ is then used to project the interval $[-1, 1]$ onto $[t-\tau, t]$. The Chebyshev meshing points can be obtained by dividing the interval $[t-\tau, t]$ into segments $[t_i, t_{i-1}]$, $(i = 1, 2, \cdots, N)$, as[8]

$$\theta_i = \frac{\tau}{2}\left[\cos\left(i\frac{\pi}{N}\right) - 1\right] \tag{59}$$

as illustrated in Fig 4, where $\tau = 1$ after the transformation made in Eq. (41).

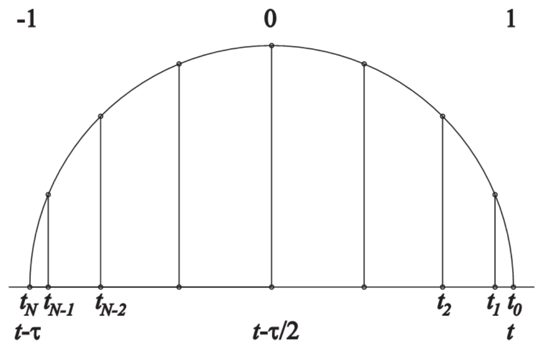

Figure 4. Chebyshev collocation points[8]

A Chebyshev spectral differentiation matrix D is defined as

$$\begin{aligned} D_{00} &= \frac{2N^2+1}{6} = -D_{NN}, \quad D_{jj} = -\frac{t_j}{2(1-t_j^2)}, \ j = 1, 2, \cdots, N-1 \\ D_{ij} &= \frac{c_i(-1)^{i+1}}{c_j(t_i - t_j)}, \ i \neq j, \ i, j = 0, 1, \cdots, N, \ c_i = \begin{cases} 2, \ i = 0, N \\ 1, \ \text{otherwise} \end{cases} \end{aligned} \tag{60}$$

Now, if equation of motion is written in the state-space form as in Eq. (45), then based on the definition for the augmented vector $\vec{\mathcal{Y}}$

$$\vec{\mathcal{Y}} = \left[\begin{array}{ccccc} \vec{z}^T(t_0) & \vec{z}^T(t_1) & \vec{z}^T(t_2) & \cdots & \vec{z}^T(t_N) \end{array}\right]^T, \quad i = 0, 1, \cdots, N \tag{61}$$

where $t_0 = t$ and $t_N = t - \tau$ from Fig. 4, then Eq. (45) can be written as

$$\dot{\vec{\mathcal{Y}}} = \mathcal{A}\vec{\mathcal{Y}}, \tag{62}$$

where[6,7]

$$\mathcal{A} = \left[\begin{array}{ccccc} \mathbf{A} & 0 & \cdots & 0 & \mathbf{B} \\ & & \frac{2}{\tau}[\mathbb{D}]^{q+1,mq} & & \end{array}\right], \tag{63}$$

where, again, $\tau = 1$, and

$$\mathbb{D}_{mq\times mq} = D_{m\times m} \otimes I_{q\times q}, \tag{64}$$

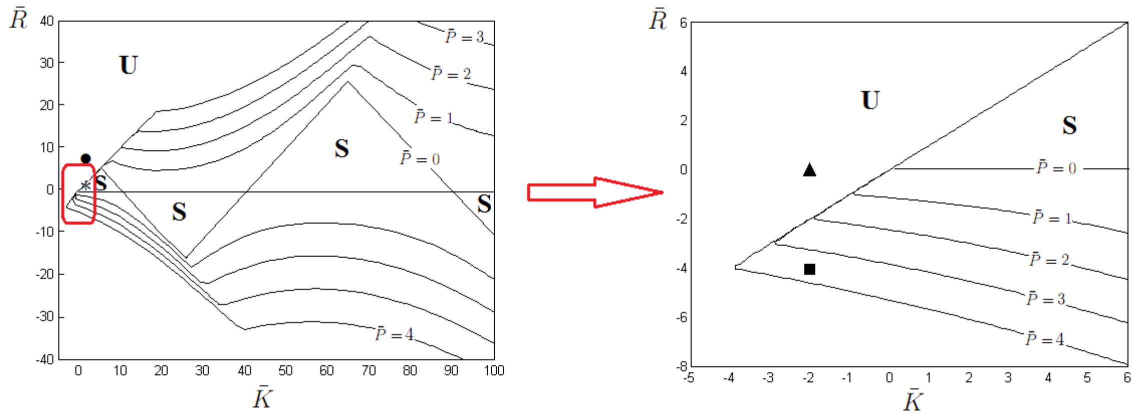

Figure 5. Stability chart in $\bar{K} - \bar{R}$ plane (Right) for $\bar{P} = 0, 1, 2, 3, 4$ obtained analytically for $\bar{P} = 0$ and numerically using ChSCTA for $\bar{P} > 0$. The $*$ and $\bullet$ shown represent the points simulated in Figs. 11 and 12, while ▲ and ■ represent the points simulated in Figs. 9 and 10, respectively.

and only rows of $\mathbb{D}$ between $q + 1$ and mq are taken into account. Based on the left half-plane analysis, the real parts of the eigenvalues of the matrix $\mathcal{A}$ in Eq. (63) determine the stability of the system such that if all eigenvalues of matrix $\mathcal{A}$ have negative real parts then system is asymptotically stable.

ChSCTA is applied to produce the Figs. 5, 6, and 7 using 85 Chebyshev collocation points in the 50×50 meshgrid. The second strategy is delay stabilization of an otherwise unstable system. The small region magnified in Fig. 5 illustrates how the added delay term stabilizes an otherwise unstable system when $K < 0$. The behavior of the system in the $\bar{K} - \bar{R}$ plane is plotted in Fig. 5 for different values of $\bar{P}$ which can be referred to as the damping of the system (43). As mentioned before, the stability boundaries do not remain as straight lines for the damped cases except for the $\bar{R} = \bar{K}$ divergence boundary which remains straight. Figure 6 shows the stable region in the $\tau - R$ diagram for $P = K = 4$ (Left), and for $P = 3$ and $K = 1$ (Right). Referring to this figure, the system is unstable for $R > 1$ when $P = 3$ and $K = 1$. In order to find the proper values of $\bar{P}$ and $\bar{K}$ which stabilize the system for some $\bar{R} > 1$ (which corresponds to $R > 1$ for $\tau = 1$), the stability is studied in the $\bar{K} - \bar{P}$ space in Fig. 7, with $\bar{R} = 2$ (Left) and $R = 6.5$ (Right), using 85 Chebyshev collocation points in a 50×50 meshgrid. As can be inferred from these plots, for $\bar{P} = \bar{K} = 4$ the MRPs of the system are in the stable region when $\bar{R} = 2$.

It should be noted that if system is just barely stable, then a small error or uncertainty in the system parameters could push the system over the stability boundary. Hence, it is often desired to design systems with some margin of error. The relative stability is compared with the stability boundary for $\bar{P} = 1$, for instance, in the $\bar{K} - \bar{R}$ plane as shown in Fig. 8. For the relative stability boundary in the figure, the spectral abscissae are assumed to be equal to $-0.01, -0.05, -0.07, -0.1$.

SIMULATION RESULTS

In this section, in order to verify the stability charts, and to study the effect of the proposed controller on the system, using MATLAB `dde23`, the time histories for arbitrarily picked stable and unstable points are produced for the time delayed system. Time histories of the system are

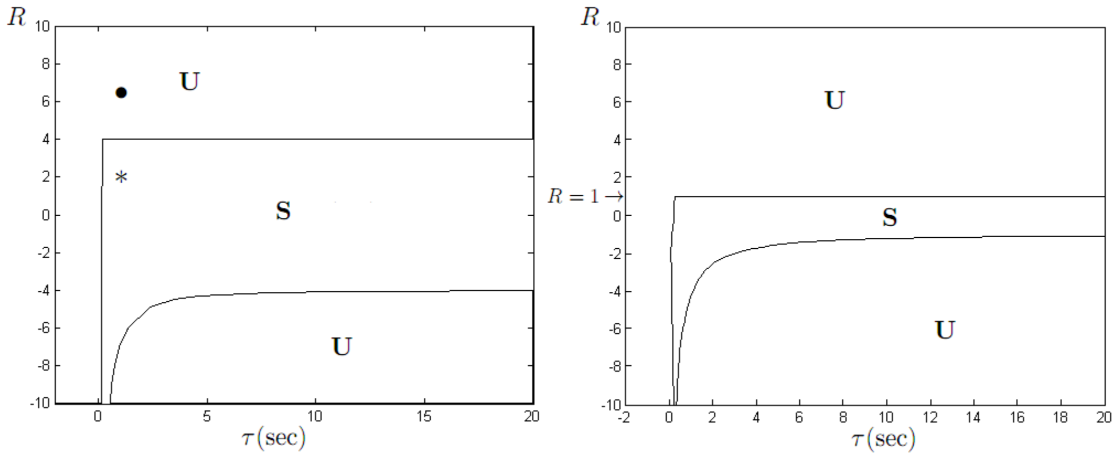

Figure 6. $\tau - R$ **plot for the closed-loop equation of the controlled system (42), S stable, U unstable;** $P = K = 4$ **(Left);** $P = 3$**,** $K = 1$ **(Right) obtained numerically using ChSCTA. The** $*$ **and** $\bullet$ **shown represent the points simulated in Fig. 11.**

further obtained for the delay-free system to compare with the literature.

In order to depict delay stabilization caused by the intentional time delay added to the system, for a negative value $K = -2$, simulations are performed for the non-delayed system as well as the delayed system with $R = -4$ and $\tau = 1$ sec. The corresponding results shown in Figs. 9 and 10 agree with the stability chart given in Fig. 5.

Two points, one from the stable region shown with $*$ and the other one from the unstable region shown with $\bullet$, are arbitrarily picked for which time series are plotted in Figs. 11 and 12. These time histories are consistent with the regions of stability and instability shown in Figs. 5, 6, and 7 for different pairs of parameter planes. The state-space form of Eq. (8) without transformation does not differ significantly from Eq. (35). Since the angular velocity response is also studied, the state-space vector $\vec{y}$ contains the angular velocity vector $\vec{\omega}$

$$\dot{\vec{y}} = \begin{pmatrix} 0_3 & I_3 & 0_3 \\ -KI_3 & -PI_3 & 0_3 \\ 0_3 & 0_3 & -PI_3 \end{pmatrix} \vec{y}(t) + \begin{pmatrix} 0_3 & 0_3 & 0_3 \\ RI_3 & 0_3 & 0_3 \\ 0_3 & 0_3 & 0_3 \end{pmatrix} \vec{y}(t-\tau) + \vec{f}(\vec{y}) \tag{65}$$

where $\vec{y} = \begin{bmatrix} \vec{\sigma}^T & \dot{\vec{\sigma}}^T & \vec{\omega}^T \end{bmatrix}^T$, as mentioned before, and the nonlinear terms are

$$\vec{f}(\vec{y}) = \begin{Bmatrix} 0_3 \\ 0_3 \\ -f\left[\vec{\omega}\vec{\omega}^T + \left(\frac{4K}{1+\sigma^2} - \frac{\omega^2}{2}\right) I_3\right]\vec{\sigma} + 4B^{-1}R\vec{\sigma}(t-\tau) \end{Bmatrix}. \tag{66}$$

First, for the same values as in the delay-free case, and the stability chart for the Eq. (8) is to be provided in the $R - \tau$ plane. The time series shown in Fig. 11 approve the stability of the angular velocity and the MRPs of the closed-loop controlled delayed system with the initial parameter values given in Table 1 using the aforementioned control law (36) for $R = 2$ and $\tau = 0.5$ sec. However, according to Fig. 6, the satellite attitude is expected to be unstable for $R > 4$, and the predictable unstable behavior is shown in Fig. 12 for the same time delay as that in Fig. 11.

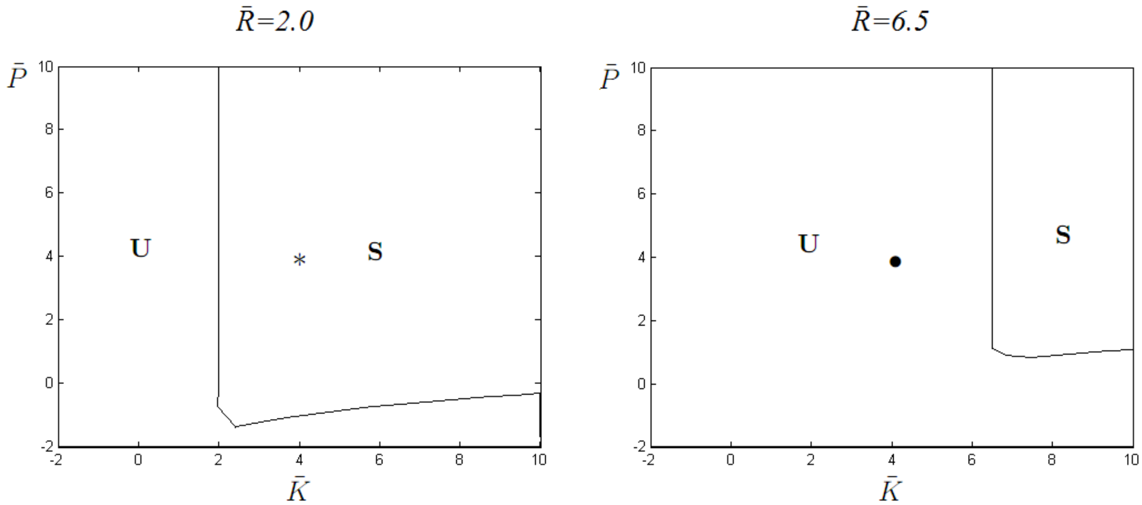

Figure 7. $\bar{K}-\bar{P}$ **plot for the closed-loop equation of the controlled system (42), S stable, U unstable, $\bar{R}$ = 2 (Left); $\bar{R}$ = 6.5 (Right) obtained numerically using ChSCTA. The $*$ and $\bullet$ shown represent the points simulated in Fig. 11.**

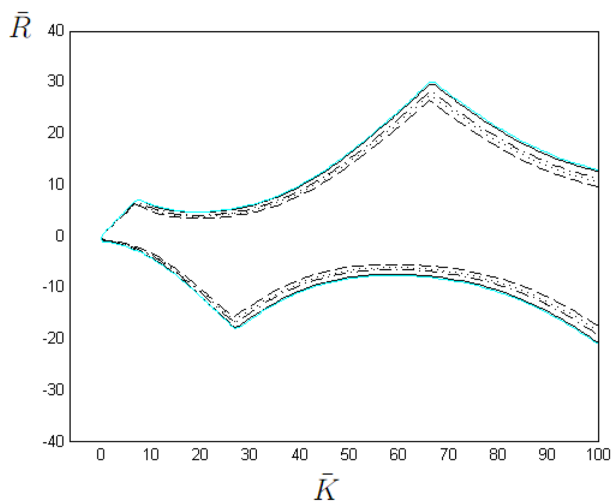

Figure 8. Relative (black) and absolute (gray) stability charts in $\bar{K}$ – $\bar{R}$ plane (Right) for $\bar{P}$ = 1. The spectral abscissae for the relative stability boundaries are -0.01 (solid line), -0.05 (dashed dotted line), -0.07 (dotted line), -0.1 (dashed line).

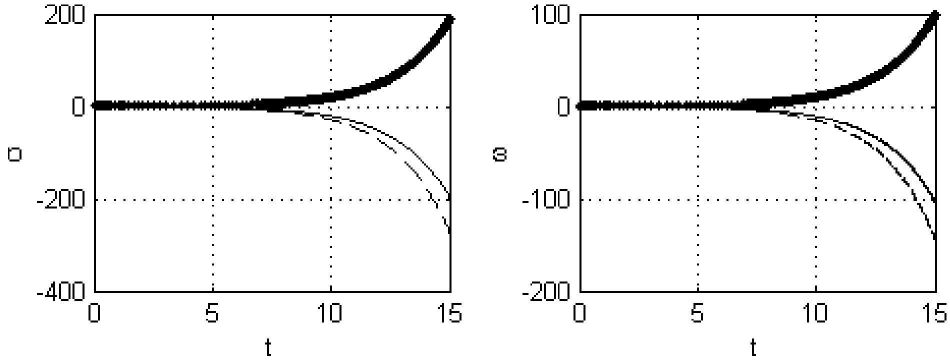

Figure 9. **Time series for the *unstable* spacecraft attitude parameters,** $\bar{P} = 4$**,** $\bar{K} = -2$**,** $\bar{R} = 0$ **without time delay indicated by ▲ in Fig. 5; MRPs (Left); angular velocity (Right). Solid (–), dashed (- -) and dotted (.) lines represent for the first, second and third components of each vector, respectively. Initial conditions are the same as those given in Table 1.**

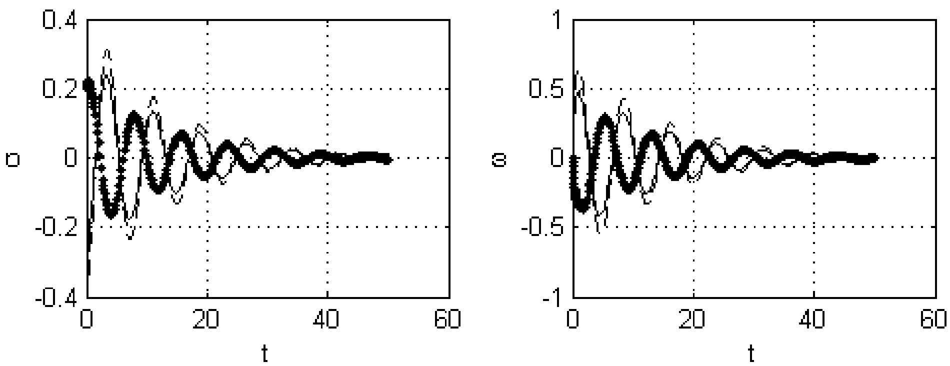

Figure 10. **Time series for the *stable* spacecraft attitude parameters,** $P = 4$**,** $K = -2$**,** $R = -4$**, and** $\tau = 1$ **indicated by ■ in Fig. 5; MRPs (Left); angular velocity (Right). Solid (–), dashed (- -) and dotted (.) lines represent for the first, second and third components of each vector, respectively. Initial conditions are the same as those given in Table 1.**

In order to verify the reliability of the simulations provided to obtain the time responses of the system, we further, by setting $R = 0$, investigate the delay-free problem corresponding to Eqs. (9) and (36), and compare the results with those obtained by Schaub and Junkins[9] for the parameter values provided in Table 1 for $P = 3$ and $K = 1$, where the two sets of simulations are found to be identical as illustrated in Fig. 13. In this figure, the time responses for the components of the attitude vector $\vec{\sigma}(t)$, the angular velocity vector $\vec{\omega}(t)$, and the control $\vec{u}(t)$ are shown for the system given by Schaub and Junkins.[9] It should be mentioned here that the norm of the MRP set was always less than one, and hence, there was no need to switch to the shadow set in the simulations. It can be seen that the aforementioned control law results in asymptotic stability of the system in a fairly small neighborhood of the origin $\left(\vec{y} = \begin{bmatrix} \vec{\sigma}^T & \dot{\vec{\sigma}}^T & \vec{\omega}^T \end{bmatrix}^T = \vec{0}\right)$.

Table 1. Parameter values[9]

Parameter	Value
J	diag$\begin{bmatrix} 30 & 20 & 10 \end{bmatrix}$ $\mathrm{kg.m}^2$
$\vec{\sigma}(t_0)$	$\begin{bmatrix} -.3 & -.4 & .2 \end{bmatrix}^T$
$\vec{\omega}(t_0)$	$\begin{bmatrix} .2 & .2 & .2 \end{bmatrix}^T$

CONCLUSIONS AND FUTURE WORK

In this paper, a nonlinear delayed control law has been introduced to acquire the desired closed-loop dynamics of a typical rigid spacecraft. As opposed to authors' other work[1] where the time delay is considered in the measurements, the time delay here has been assumed to be in the actuators. Two strategies are considered. In the first strategy, one actuator is delay-free, while the other one has time delay. Delay stabilization is another strategy, where intentional time delay is introduced into the actuator in order to stabilize the closed-loop dynamics which would be unstable without delay. The stability boundaries are obtained analytically for the undamped delayed closed-loop system which is known as the Hsu-Bhatt-Vyshnegradskii stability chart, where the stability regions appear as triangles in which the number of unstable characteristic exponents is zero. Stability boundaries, however, do not remain as straight lines, for the damped system, nor can they be investigated analytically, and hence ChSCTA has been implemented instead to obtain the stability boundaries for the damped case. MATLAB `dde23` has been applied further to obtain the time histories of the system which have been in agreement with the stability charts. Finally, in order to verify the controller, the time series obtained for the controlled delay-free system are compared to those in the literature.

This work hopes to be a first step toward further understanding the following important issues. First, the control gains P and K are selected arbitrary in this study. In control design, it is usually important, however, to design the gains of the closed-loop dynamics for *specified performance* such as critical damping. Second, unmodeled external torques due to effects such as atmospheric drag or bearing friction can cause steady state errors which should be eliminated or diminished by *adding an integral feedback term*. We are also looking into ways to extend the method introduced in the present work to do the *attitude tracking problem*.

ACKNOWLEDGMENTS

Financial support from the National Science Foundation under Grant Nos. CMMI-0900289 and CMMI-1131646 is gratefully acknowledged.

REFERENCES

[1] E. Samiei, M. Nazari, E. Butcher, and H. Schaub, "Delayed Feedback Control of Rigid Body Attitude using Neural Networks and Lyapunov-Krasovskii Functionals," *AAS/AIAA Spaceflight Mechanics Meeting, Charleston, SC, Paper No. 12-168*, Jan. 29–Feb. 2, 2012.

[2] C. Hall, P. Tsiotras, and H. Shen, "Tracking Rigid Body Motion Using Thrusters and Momentum Wheels," *Journal of the Astronautical Sciences*, Vol. 50, 2002, pp. 311–323.

[3] P. Tsiotras, H. Shen, and C. Hall, "Satellite Attitude Control and Power Tracking with Energy/Momentum Wheels," *Journal of Guidance, Control, and Dynamics*, Vol. 24, 2001, pp. 23–34.

[4] A. Chunodkar and M. Akella, "Attitude Stabilization with Unknown Bounded Delay in Feedback Control Implementation," *Journal of Guidance, Control, and Dynamics*, Vol. 34, 2011, pp. 533–542.

[5] A. Ailon, R. Segev, and S. Arogeti, “A Simple Velocity-Free Controller for Attitude Regulation of a Spacecraft with Delayed Feedback,” *IEEE Transactions on Automatic Control*, Vol. 49, 2004, pp. 125–130.

[6] E. Butcher and O. Bobrenkov, “On the Chebyshev Spectral Continuous Time Approximation for Constant and Periodic Delay Differential Equations,” *Communications in Nonlinear Science and Numerical Simulation*, Vol. 16, 2011, pp. 1541–1554.

[7] O. Bobrenkov, E. Butcher, and B. Mann, “Application of the Liapunov-Floquet Transformation to Differential Equations with Time Delay and Periodic Coefficients,” *Journal of Vibration and Control, in press*.

[8] O. Bobrenkov, M. Nazari, and E. Butcher, “On the Analysis of Periodic Delay Differential Equations with Discontinuous Distributed Delays,” *Journal of Computational and Nonlinear Dynamics, in press*.

[9] H. Schaub and J. Junkins, *Analytical Mechanics of Space Systems*. Reston, Virginia: AIAA, 2009.

[10] R. Paielli and R. Bach, “Attitude Control with Realization of Linear Error Dynamics,” *Journal of Guidance, Control, and Dynamics*, Vol. 16, 1993, pp. 182–189.

[11] T. Insperger and G. Stépán, *Semi-Discretization for Time-Delay Systems, Stability and Engineering Applications*. New York: Springer, 2011.

[12] G. Stépán, *Retarded Dynamical Systems: Stability and Characteristic Functions*. Great Britain: Longman Scientific and Technical, 1989.

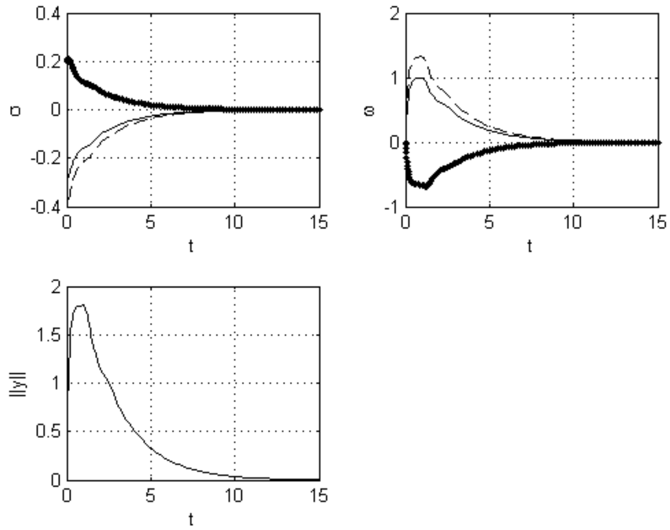

Figure 11. Time series for the *stable* spacecraft attitude parameters, $P = 8$, $K = 16$, $R = 8$, $\tau = 0.5$ sec for the stable location indicated by $*$ in Figs. 5, 6, and 7; MRPs (Top-Left); angular velocity (Top- Right); Euclidean norm of the assembled satellite attitude vector $\left[\vec{\sigma}^T, \vec{\omega}^T\right]^T$ (Bottom). Solid (–), dashed (- -) and dotted (.) lines represent for the first, second and third components of each vector, respectively. Initial conditions are the same as those given in Table 1.

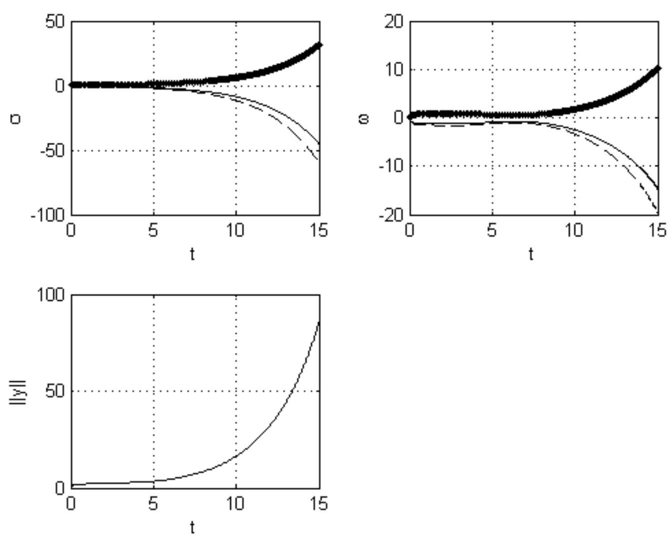

Figure 12. Time series for the unstable spacecraft attitude parameters, $P = 8$, $K = 16$, $R = 26$, $\tau = 0.5$ sec for the unstable location indicated by $\bullet$ in Figs. 5, 6, and 7; MRPs (Top-Left); angular velocity (Top-Right); Euclidean norm of the assembled satellite attitude vector $\left[\vec{\sigma}^T, \vec{\omega}^T\right]^T$ (Bottom). Solid (–), dashed (- -) and dotted (.) lines represent for the first, second and third components of each vector, respectively with initial conditions given in Table 1.

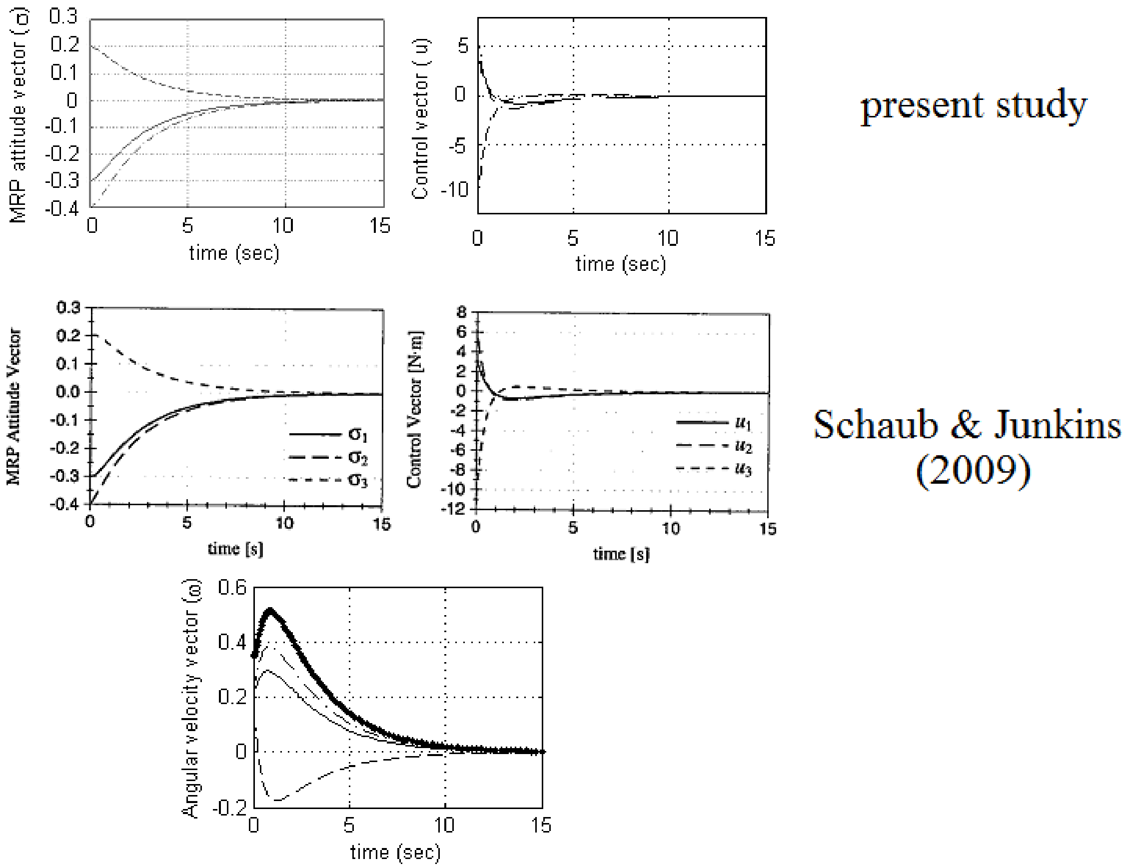

Figure 13. **Time history of $\vec{\sigma}$ (first row, left), $\vec{u}$ (first row, right), and $\vec{\omega}$ (third row) with dotted lines (.) representing the norms, and solid lines (–), dashed dotted lines (-.), and dashed lines (- -) representing the first, second and third components of each vector, respectively, as compared to $\vec{\sigma}$ (second row, left) and $\vec{u}$ (second row, right) given by Schaub and Junkins[9] .**